Polymer Chemistry
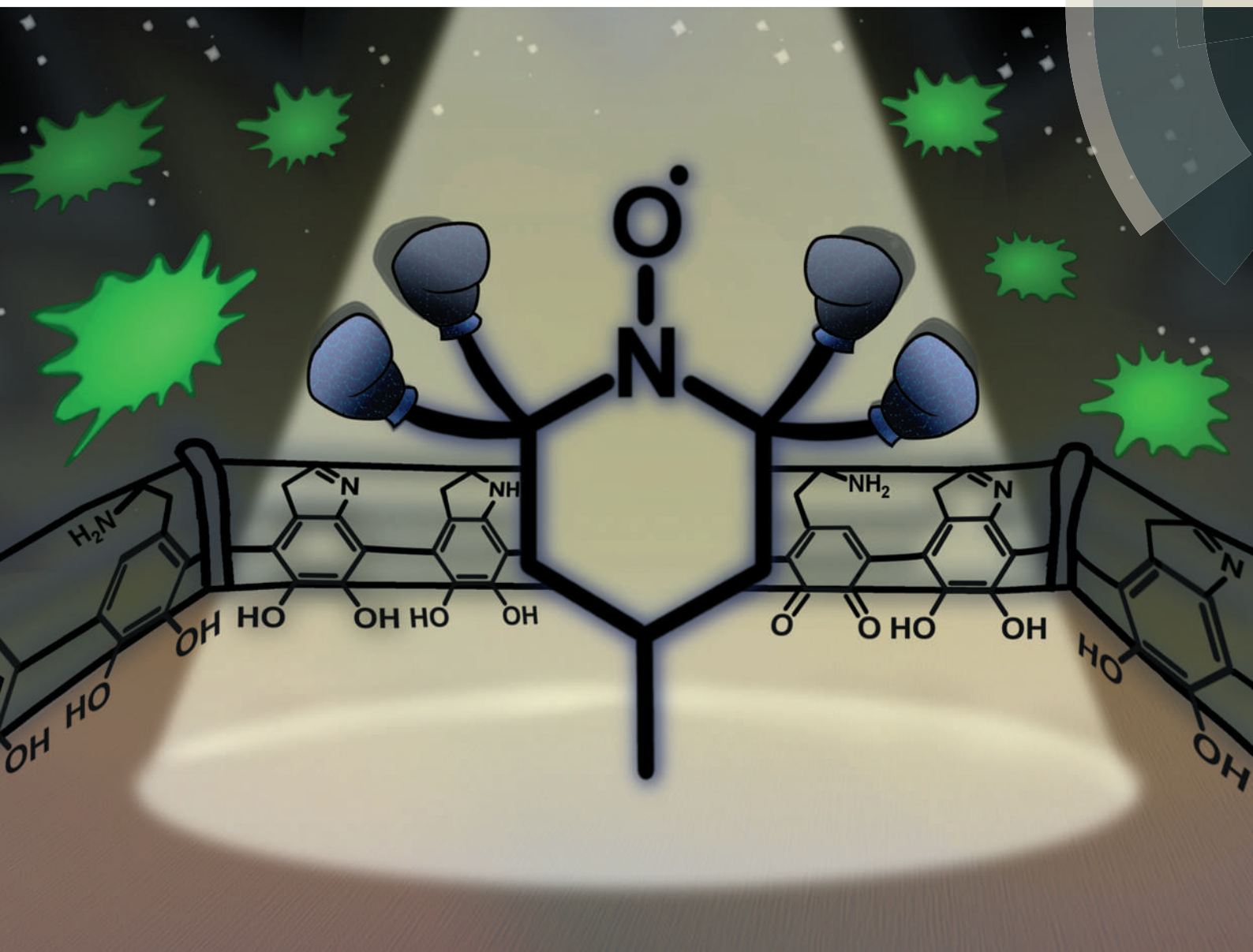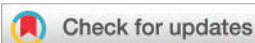
ROYAL SOCIETY
OF **CHEMISTRY** | Celebrating
IYPT 2019

PAPER
Robert E. W. Hancock, Christopher Barner-Kowollik,
Kathryn E. Fairfull-Smith *et al.*
Controlling biofilm formation with nitroxide functional
surfaces

Controlling biofilm formation with nitroxide functional surfaces†

Hendrik Woehlk,[a,b,c] Michael J. Trimble, [ID][c] Sarah C. Mansour,[c] Daniel Pletzer, [ID][c] Vanessa Trouillet, [ID][d,e] Alexander Welle, [ID][e,f] Leonie Barner, [ID][a,g] Robert E. W. Hancock,*[c] Christopher Barner-Kowollik [ID] *[a,b,g] and Kathryn E. Fairfull-Smith [ID] *[a]

Bacterial biofilm formation on medical devices is a threat to healthcare systems worldwide as bacteria within a biofilm are more resistant to standard antimicrobial therapies. Herein, we introduce a nitroxide-based anti-biofilm coating strategy, which is specifically designed to prevent biofilm formation of Gram-negative patho-gens such as *Pseudomonas aeruginosa*. Nitroxide-decorated hydroxyapatite surfaces were readily prepared in an aqueous dip-coating procedure using a nitroxide-functionalized catecholamine as a polymerizable coating agent. Additional spatial control over the polymer surface deposition on titanium was gained by applying a photolithographic coating setup. All nitroxide-coated surfaces exhibited excellent antibiofilm pro-perties toward PA14 surface colonization as biofilm formation was completely suppressed. Importantly, the surrounding adhesive polymer matrix did not interfere with the nitroxide-characteristic antibiofilm pro-perties. The herein introduced platform technology represents a bioinspired and versatile coating approach, offering a safe and prophylactic avenue to combat biofilm contamination on a variety of surfaces.

Introduction

Biofilms are surface-attached, multicellular, and highly-structured bacterial communities embedded in a self-produced extracellular protective matrix.[1–3] They evolve from initial planktonic surface attachment and microcolonization, followed by maturation toward large bacterial aggregates, which are highly adaptive in hostile environments. Bacterial proliferation occurs on all types of surfaces including medical devices and implants, and critically, the enclosed bacteria within a biofilm are highly resistant toward external environmental stresses (*e.g.*, antibiotics). Consequently, biofilms are of tre-mendous concern in hospitals worldwide accounting for many chronic and persistent infections as well as device-associated infections.[1,2,4] The challenge of pathogenic biofilms is that once a biofilm has formed on a surface, it is extremely difficult to eradicate the sessile bacteria using standard antimicrobial agents.[5] Instead, the biofilm often acts as a nidus for acute and persistent infections in the human body. If the source is from contaminated indwelling devices, they often have to be sur-gically removed.[6] To date, modern bactericidal drug design does not specifically appreciate and target bacteria existing in a biofilm, and the development of potent antibiofilm agents is still in the early stages.[7–9] Among them, nitroxides, stable free organic radicals with an unpaired electron delocalized over the nitrogen–oxygen bond, have only been ascribed a marginal role as biofilm dispersing agents.[10,11] The nitroxide's mode of action is referred to the structurally mimicking properties of nitric oxide (NO), which is an important signalling molecule in biofilm regulation mediating, for instance, biofilm dispersal events.[12–15] Using nitr-oxides, however, can overcome key drawbacks attributed to the nature of NO and NO donor molecules including the persistence of the nitroxyl radical, safe handling, and many existent chemical modification strategies including the design of nitroxide conju-gates with polymeric drug carriers[16,17] or antibiotics.[18]

Preventive strategies to combat bacterial proliferation on surfaces typically encompass the (physico-)chemical manipu-

[a]School of Chemistry, Physics and Mechanical Engineering, Queensland University of Technology (QUT), 2 George Street, Brisbane, QLD 4000, Australia. E-mail: christopher.barnerkowollik@qut.edu.au, k.fairfull-smith@qut.edu.au

[b]Macromolecular Architectures, Institut für Technische Chemie und Polymerchemie, Karlsruhe Institute of Technology (KIT), Engesserstr. 18, 76131 Karlsruhe, Germany

[c]Department of Microbiology and Immunology, Center for Microbial Diseases and Immunity Research, University of British Columbia, Vancouver, BC V6T 1Z4, Canada. E-mail: bob@hancocklab.com

[d]Institute for Applied Materials (IAM-ESS), Karlsruhe Institute of Technology (KIT), Hermann-von-Helmholtz-Platz 1, 76344 Eggenstein-Leopoldshafen, Germany

[e]Karlsruhe Nano Micro Facility (KNMF), Karlsruhe Institute of Technology (KIT), Hermann-von-Helmholtz-Platz 1, 76344 Eggenstein-Leopoldshafen, Germany

[f]Institute of Functional Interfaces (IFG), Karlsruhe Institute of Technology (KIT), Hermann-von-Helmholtz-Platz 1, 76344 Eggenstein-Leopoldshafen, Germany

[g]Institute for Future Environments, Queensland University of Technology (QUT), 2 George Street, Brisbane, QLD 4000, Australia

†Electronic supplementary information (ESI) available: Experimental details, characterization methods and supplemental data. See DOI: 10.1039/c9py00690g

lation of the underlying (afflicted) material, such as antifouling (*e.g.*, inhibition of initial bacterial surface attachment using fluoropolymer- or poly(ethylene glycol)-based coatings)[19,20] or antimicrobial coating strategies.[21–23] However, the latter approach, in particular, has to be seen critically in terms of the 'antimicrobial resistance crisis'[24] and furthermore, dead cells present on the surface typically mitigate the local biocidal effect for approaching bacteria.[21] Antibiofilm coatings with the purpose to exclusively regulate biofilm formation on surfaces by actively promoting the planktonic lifestyle of bacteria still remain elusive as a strategy to combat biofilm surface contaminations. Critically, the ubiquity of biofilms on all types of surfaces ideally requires a versatile surface coating technique, which proceeds irrespectively of the underlying material properties.[25,26] A universal coating platform has emerged using polycatechols as bioderived interfacial modifier.[27,28] The use of catechol-functionalized coating agents, for instance, has its inspiration from marine mussels and their efficient adhesion system based on 3,4-dihydroxyphenylalanine (DOPA)- and lysine-enriched mussel foot proteins, which allow them to adhere to virtually all types of materials while withstanding rough marine conditions.[28,29] Applied to modern chemistry and material sciences,[30] catecholamines have been introduced as great biomimicking coating agents generating highly adhesive polymer networks upon aqueous, aerobic polymerization.[31] Herein, we exploited this versatile and widely applicable surface coating strategy for the fabrication of nitroxide functional polymer coatings and examined the potency of nitroxide-decorated surfaces against *Pseudomonas aeruginosa* surface colonization and biofilm maturation. Selected materials were coated with thin polymer films during the oxidative polymerization of a nitroxide functional catecholamine using its inherent adhesive properties upon polymerization. Our antibiofilm coating approach specifically targets the prevention of biofilm formation on surfaces as a key strategy to reduce bacterial biofilm contaminations in hospitals.

Results and discussion

Fabrication of antibiofilm polymer coatings

The substrate-independent polymer coating strategy is designed as a highly adaptable research platform for the facile immobilization of various functional groups (*e.g.*, nitroxides) to a variety of (medically-relevant) materials. Our approach enables the precise delivery of bioactive moieties to the substrate interface aiming to study their effect on bacterial proliferation and biofilm formation on surfaces. Practically, the simple dip-coating procedure only requires a catecholamine-based functional monomer, which polymerizes under aqueous, aerobic conditions yielding a polycatecholic network with strong, universal adhesive properties—in close analogy to the catechol-enriched bioadhesion system of marine mussels.

The coating agent equipped with a 2,2,6,6-tetramethyl-piperidine-1-oxyl (TEMPO)-derived functional group has been previously introduced by our group.[32] In brief, 4-amino-TEMPO was amide-linked to 3,4-dihydroxy-L-phenylalanine (L-DOPA) under implementation of standard *tert*-butyldimethylsilyl (TBDMS) ether and *tert*-butyloxycarbonyl (Boc) protection group chemistries.[33] The quantitative cleavage of both protecting groups was carried out under acidic conditions. Simultaneously, the TEMPO free radical moiety of **4** was converted to the corresponding hydroxylamine hydrochloride salt (Fig. 1a). The oxidation and reformation of nitroxide persistent radicals was achieved during the aerobic polymerization of **4** and is discussed in detail elsewhere.[32]

In addition to the nitroxide-functionalized DOPA derivative, a reference coating agent was introduced bearing a cyclohexyl (Cy) moiety attached to the polymerizable catecholamine unit with the aim to study potential biological side effects stemming from the surrounding adhesive polymer matrix in the absence of biofilm-active nitroxides. Coating agent **5** was prepared according to the general synthetic protocol depicted in Fig. 1a using cyclohexylamine as a 4-amino-TEMPO substitute. Compound **5** was isolated in high yield (82% in total) and fully characterized by ^{1}H and ^{13}C nuclear magnetic resonance (NMR) spectroscopy (refer to Fig. S1 and S2†) as well as high-resolution mass spectrometry (HRMS).

The oxidative polymerization of coating agents **4** or **5** (40 mM), respectively, was performed under optimized conditions using a slightly alkaline Tris-HCl buffer system (100 mM, pH 9.25) and atmospheric oxygen as an oxidant (Fig. 1b).[34] Initialized by the catechol oxidation, highly reactive *o*-quinoic intermediates, such as aminochrome-like structures were formed, which further underwent complex intramolecular as well as intermolecular oxidative reaction cascades yielding a structurally heterogeneous polymer system, where 5,6-dihydroxyindole was identified as a key structural element constituting the polymer backbone.[31,32,35–37] A representative but simplified structure of the adhesive polymer backbone is depicted in Fig. 1b with the corresponding key functional groups (R = TEMPO or Cy) expressed in the polymer side chains. The immersed substrates, such as hydroxyapatite (HA) discs (tooth enamel model)[38] with excellent biofilm surface compatibilities, were typically immersed into the coating solution for 24 h yielding nitroxide (**B**) or cyclohexyl (**C**) decorated surfaces.

Characterization of polymer-coated hydroxyapatite surfaces

The polymer coatings with either TEMPO (**B**) or cyclohexyl (**C**) functional groups immobilized onto the surface were carefully analyzed by X-ray photoelectron spectroscopy (XPS) and time-of-flight secondary ion mass spectrometry (ToF-SIMS). Both coatings showed almost identical chemical compositions with respect to the obtained high-resolution C 1s XP spectra (Fig. 2a). The C 1s spectra were deconvoluted into three main components, which corresponds to the complex poly(DOPA amide) system and various incorporated but structurally closely related building blocks constituting the polymer backbone (refer to Fig. 1b). However, the existence of N-heterocyclic TEMPO residues on surface **B** resulted in a more pronounced
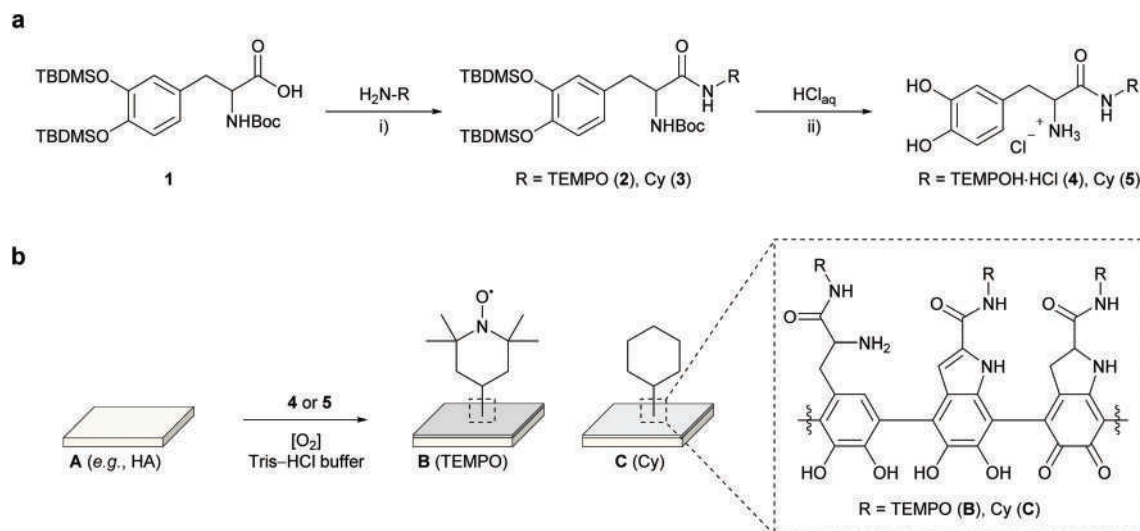
Fig. 1 Manufacturing of functional polymer coatings. (a) General synthetic pathway for the preparation of catecholamine-based coating agents bearing TEMPO-derived (**4**) or Cy (**5**) residues. Compound **4** was isolated as the corresponding hydroxylamine hydrochloride salt, which is prone to oxidize under aqueous, aerobic conditions regenerating the nitroxide free radical. (i) EDC·HCl, DMAP, dry DCM, 24 h, a.t., (ii) aq. 6 M HCl, MeOH, 6 h, 0 °C → r.t. (b) Coating strategy based on the aerobic polymerization of **4** or **5** (40 mM) in Tris–HCl buffer (100 mM, pH 9.25). The *in situ* polymer film formation on HA was performed for 24 h. A simplified structure of the (undefined) adhesive polymer backbone is displayed.
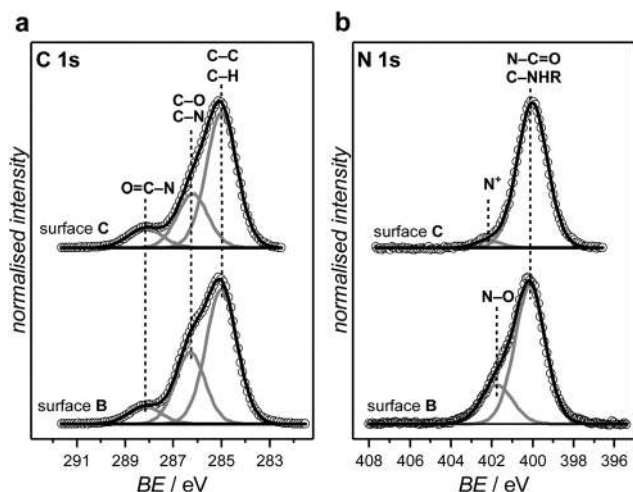

Fig. 2 XPS characterization of polymer coatings. (a) C 1s and (b) N 1s XP spectra of surfaces **B** (TEMPO) and **C** (Cy).

C–N peak (at 286.2 eV) compared to surface **C** with only homo-cyclic polymer side chains. In addition, TEMPO-derived ami-noxyl functional groups on surface **B** were unambiguously confirmed by the N–O characteristic peak at 401.8 eV in the corresponding N 1s XP spectrum (Fig. 2b, bottom row). The dominant peak at 400.1 eV was hereby assigned to various N-containing poly(DOPA amide) structures constituting the polymer backbone. The Cy-decorated surface **C**, on the contrary, only showed a peak of weak intensity adjacent to the main peak in the N 1s spectrum which, most likely, indicates protonated amine species existent in the polymer system. ToF-SIMS analysis further confirmed the polymer composition

of **B** and **C** with poly(DOPA) characteristic [CN]⁻ fragments detected on both surfaces and TEMPO-characteristic [NO]⁻ fragments exclusively detected on surface **B** (refer to Fig. S3†).

P. aeruginosa biofilm studies

The bacterial biofilm studies were performed with *P. aeruginosa*, a Gram-negative opportunistic pathogen with clinical and economic burden in healthcare systems world-wide. Furthermore, *P. aeruginosa* has become a model microorganism in biofilm research, including recent studies using nitroxides and nitric oxide as potent antibiofilm agents.[10,12,13,39] A GFP-labelled PA14 strain was employed for the direct visualization of surface-adherent biomass after biofilm cultivation, which was carefully assessed by confocal laser scanning microscopy (CLSM) (Fig. 3). Coated and uncoated hydroxyapatite substrates **A–C** were colonized with PA14 and cultivated under flow conditions using basal medium 2 (BM2) as a minimal medium.[10] The substrates were placed adjacently within the same flow cell chamber prior to PA14 inoculation (orientation did not matter), and biofilm cultivation was performed for 72 h.

Comparison of the green fluorescence response on surfaces **A–C** unambiguously demonstrates the antibiofilm properties stemming from surface-immobilized nitroxides with representative confocal images displayed in Fig. 3. Uncoated HA (Fig. 3, left image) showed a widespread PA14 biofilm surface coverage with matured biofilm structures spotted on the surface (some of them exceed 15 μm in all three dimensions). Thus, surface **A** served as a suitable control experiment for the direct comparison with polymer-coated analogous surfaces. The confocal microscopy image of the TEMPO-functionalized surface **B** only showed a weak fluorescence response indicating
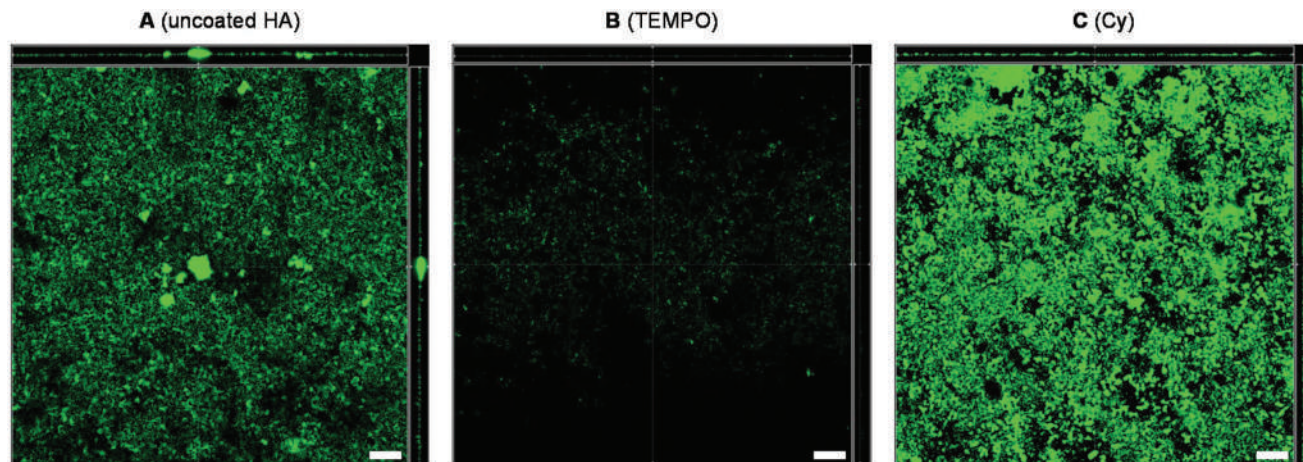
Fig. 3 *P. aeruginosa* biofilm cultivation on unmodified and polymer–coated hydroxyapatite surfaces. Uncoated (**A**), nitroxide polymer–coated (**B**), and cyclohexyl polymer–coated (**C**) surfaces were exposed to PA14 surface colonization for 72 h in a flow cell system at 37 °C. Biofilm surface coverage of a GFP-tagged PA14 strain was assessed by CLSM. The scale bars represent 50 μm in length. Each panel shows the *xy*, *yz* and *xz* dimensions.

that biofilm formation was suppressed on the modified surface (Fig. 3, centered image). Instead, only single cells and minor microcolonies were present on surface **B**. The second polymer coating system bearing Cy functional polymer side groups (surface **C**) was completely ineffective against bacterial proliferation and biofilm formation. As shown in Fig. 3 (right image), the surface was almost entirely covered by a biofilm, even with a stronger fluorescence response compared to the biomass adherent on the uncoated surface **A**. Thus, the anti-biofilm effect was not preserved after substituting nitroxide functional groups by cyclohexyl residues within the adhesive polymer matrix. Yet, we assume that the biofilm preventing mode of action of surface-conjugated nitroxides is only contact dependent as this type of coating is not equipped with any bacteria repelling properties targeting to suppress initial surface attachment of bacteria, which is typically the case when poly (ethylene glycol) polymer brushes or fluoropolymers are employed as antifouling coatings.[21] It is likely that biofilm formation was inhibited as a result of the NO mimicking character of nitroxides, promoting the planktonic mode of growth of bacteria by interfering with the bacterial cell–cell communication system.[10] As the adhesive polymer system is mainly composed of oligomeric strands (*e.g.*, hexamers),[32] which are supramolecularly assembled by various non-covalent interactions, is it assumed that the nitroxide's mode of action at the substrate interface is enhanced by the inherent dynamic character of the surrounding polymer matrix for better interaction with approaching bacteria.

Similar observations were made when nitroxide-coated titanium surfaces were exposed to PA14 biofilm cultivation showing a complete inhibition of bacterial surface colonization with absolutely no green fluorescent biomass attached to the surface (refer to Fig. S4† top row). Furthermore, additional antimicrobial eradication experiments using ciprofloxacin (a standard antibiotic for Gram-negative *P. aeruginosa*) at its minimum inhibitory concentration (MIC = 320 ng ml^{-1})[39]

clearly failed to eradicate the bacteria within a biofilm (cultivated on titanium) due to its recalcitrance to antibiotics at MIC concentrations. The nitroxide-decorated surface **B**, however, remained free from any bacterial proliferation indicating its potential as a prophylactic coating strategy to reduce the use of (biofilm-ineffective) antibiotics after biofilm contamination has occurred (refer to Fig. S4† bottom row).

Photolithographic control of biofilm formation

The versatile polycatecholic coating system was further exploited for spatially controlled surface immobilization of nitroxide-containing polymers onto titanium substrates generating antibiofilm domains with submillimeter resolution (Fig. 4). The photolithographic coating setup was simply triggered by UV-light ($\lambda_{\max}$ = 313 nm) for the accelerated formation of reactive oxygen species (ROS) inducing the catechol oxidation and subsequent catecholamine polymerization of **4** (Fig. 4a).[40] Careful optimization of the coating parameters (5 mM of **4** in 10 mM Tris-HCl buffer, pH 8.5) resulted in a suppression of the polymerization when the reaction was performed in the dark. Contrary to this, a rapid polymer formation was observed when the coating solution was exposed to UV light. The light-dependent build-up of reactive *o*-quinoic intermediates and oligomers, for instance, was monitored by UV–vis spectroscopy (Fig. 4b). With proceeding polymerization time and under UV exposure, a broad shoulder at higher wavelengths emerged adjacent to the catechol-assigned UV band (λ = 280 nm) indicating that complex oxidative reaction cascades of the catechol group have occurred.[32] This observation was less pronounced when the reaction was performed in the dark with only minor changes in the recorded UV–vis spectra (Fig. 4b, right panel). Noteworthy, UV irradiation did not negatively impact the hydroxylamine oxidation and nitroxide free radical formation during polymerization of **4** (refer to Fig. S5†). At the same time, the light-dependent polymer film formation on silicon (employed as a model substrate) was
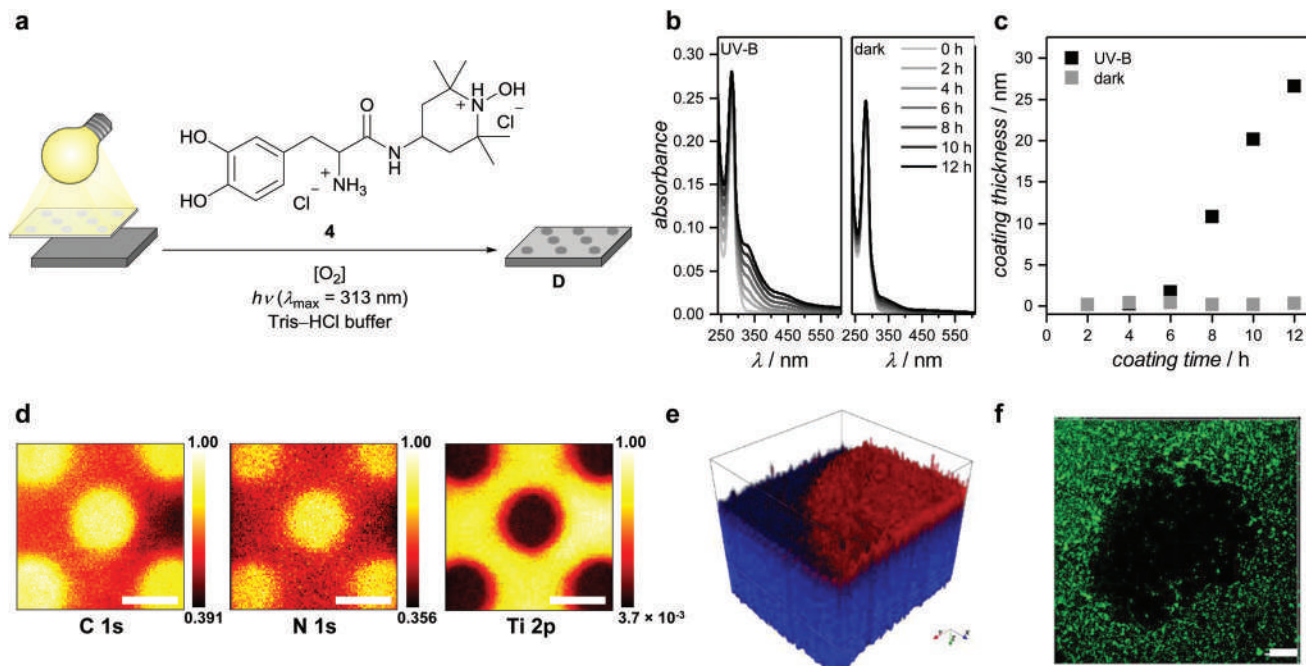
Fig. 4 Light-induced polymer film formation on surfaces generating spatially confined antibiofilm domains. (a) Synthetic route for the photo-polymerization of **4** concomitant with spatially controlled polymer surface immobilization onto titanium substrates. Monomer **4** was dissolved in Tris–HCl buffer (10 mM, pH 8.5). The immersed titanium substrates (1 × 1 cm^2) was covered by a dotted shadow mask (Ø 1 mm pinholes) beforehand. UV irradiation (λ_{max} = 313 nm) was performed for 12 h at room temperature. (b) UV–vis spectroscopic monitoring of catechol oxidation and cat-echolamine polymerization of **4** under UV-B irradiation (left panel) and in the dark (right panel). (c) Coating thickness of polymer films deposited on silicon substrates under UV irradiation (black squares) and in the dark (grey squares), determined by spectroscopic ellipsometry. (d) C 1s, N 1s, and Ti 2p XPS images of polymer-patterned surface **D**. The scale bars represent 1 mm in length. (e) 3D ToF-SIMS rendering of surface **D** with underlying titanium illustrated in blue and a quarter of one nitroxide polymer spot deposited on the surface (depicted in red). Polymer signals (red) are the sum of $[C_2H_5]^+$, $[C_3H_5]^+$, $[C_2H_5N]^+$, and $[NH_4]^+$ fragments. Titanium signals (blue) derived from the sum of all Ti isotopes. The x and y range is 500 μm (black box), the z range is not to scale. (f) *P. aeruginosa* biofilm cultivation on nitroxide patterned titanium surface **D**. Surface **D** was exposed to a GFP-labelled PA14 strain for 72 h under static biofilm growth conditions at 37 °C. The confocal image was obtained through 3 × 3 rastering along the xy dimension with approx. 16 μm depth profile (indicated in yz and xz side panels). The scale bar represents 200 μm in length.

investigated by spectroscopic ellipsometry (Fig. 4c). A rapid increase of the coating thickness was observed after reactive oligomeric building blocks have been formed in the initial stage of polymerization (between 0 and 6 h). In the dark, polymer film formation on silicon was completely suppressed within the first 12 h of polymerization as the concentration of oxidized (reactive) intermediates of **4**—required for the construction of the adhesive polymer matrix—was constantly maintained at low levels (refer to Fig. 4b). Thereafter, the same coating conditions were applied for the spatially resolved surface immobilization of nitroxide functional polymers using monomer **4** as a coating agent and a photolithographic experimental setup. Titanium flat substrates (1 × 1 cm^2, covered by a dotted shadow mask with Ø 1 mm pinholes) were immersed into the coating solution for 12 h under continuous UV exposure.

The successful polymer film formation with spatial resolution was carefully assessed by advanced XPS and ToF-SIMS imaging techniques (Fig. 4d and e). The XPS mapping of surface **D** (over a 3 × 3 mm^2 area) clearly showed the precise polymer surface pattern in correspondence to the employed dotted shadow mask. Strong polymer-derived C 1s and N 1s

XPS signals were predominantly detected in circular areas which have been exposed to UV irradiation. Simultaneously, no Ti 2p XPS signals (stemming from the underlying Ti substrate) were detected in those areas supporting the successful localized polymer film formation on surface **D** (Fig. 4d). The surrounding areas, which have been shielded from UV irradiation by the shadow mask, showed less pronounced C 1s and N 1s XPS signals, and on the contrary, intense substrate-derived Ti 2p XPS signals. The omnipresent polymer-derived C 1s and N 1s signals on surface **D**, however, imply that polymer surface deposition has taken place over the entire surface. Furthermore, this observation indicates that the use of UV light only controls the localized build-up of reactive and propagating oligomer building blocks. However, it does not impact the inherent and universal adhesive properties of the growing poly(DOPA amide) chains freely diffusing in solution and thus, randomly depositing onto the entire surface to a minor extent. Nevertheless, a clear coating gradient between UV-exposed and UV-shielded areas was visualized by XPS with polymer thicknesses ≥10 nm at UV-exposed areas due to the absence of substrate-specific Ti 2p signals. An in-depth XPS characterization study with recorded high-resolution XP spectra

at well-defined positions corresponding to polymer-conjugated and nonconjugated areas is presented in the ESI (refer to Fig. S6†). Further evidence of a successful polymer film formation with spatial precision was given by ToF-SIMS (Fig. 4e). A quarter of one polymer spot was clearly accentuated from the underlying Ti substrate employing the dynamic SIMS mode (over a 500 × 500 μm² area) for the visualization of polymer-characteristic $[C_2H_5]^+$, $[C_3H_5]^+$, $[C_2H_5N]^+$, and $[NH_4]^+$ fragments (illustrated in red, Fig. 4e). The imaging of the Ti substrate (depicted in blue) was achieved *via* the sum of all Ti isotopes. The detailed ToF-SIMS characterization pathway toward the 3D rendered image is explained in the ESI (refer to Fig. S7–S10†).

The polymer patterned surface **D** was exposed to PA14 surface colonization for 72 h under static biofilm growth conditions for the biological evaluation of the nitroxide-stemming antibiofilm surface properties in direct comparison to the surrounding unmodified areas. A clear difference in biofilm surface coverage between polymer-coated and uncoated areas was observed on surface **D** with a representative confocal image depicted in Fig. 4f showing one circular polymer spot (Ø 1 mm). The uncoated peripheral area was completely covered by a mature biofilm (green fluorescent) and contrary to that, the polymer-coated circular area showed resistance toward *P. aeruginosa* biofilm formation (centered in Fig. 4f).

Conclusions

In this study, we introduced a simple and versatile polymer coating strategy to (spatially) control *Pseudomonas aeruginosa* biofilm formation on a variety of surfaces. Thin, nitroxide-containing polymer films were immobilized on hydroxyapatite and titanium surfaces exploiting the universal bioadhesive properties of a TEMPO-functionalized catecholamine after its aerobic polymerization in aqueous solution at room temperature. This coating procedure was carried out under extremely mild conditions with no chemical additives and the need of an elaborate experimental setup. Furthermore, a photolithographic coating approach enabled the manufacturing of spatially-defined antibiofilm patterns with a clear gradient in polymer thickness between UV-exposed and UV-shielded areas as shown by XPS and ToF-SIMS measurements.

The careful evaluation of biofilm formation on various uncoated and polymer-coated substrates clearly demonstrated that nitroxide-decorated surfaces were significantly less prone to bacterial surface colonization and biofilm maturation. Importantly, this antibiofilm effect was unambiguously assigned to the covalently embedded nitroxide functional groups with no (synergistic) contribution derived from the surrounding adhesive polymer matrix. In conclusion, our polymer coating platform was specifically designed to coat and display nitroxides on various surfaces in order to carefully evaluate their antibiofilm properties. This coating approach offers a safe and efficient strategy to reduce biofilm contamination on surfaces and thus, to combat biofilm-related infections in the hospital.

Conflicts of interest

There are no conflicts to declare.

Acknowledgements

References

1 L. Hall-Stoodley, J. W. Costerton and P. Stoodley, *Nat. Rev. Microbiol.*, 2004, **2**, 95–108.
2 J. W. Costerton, P. S. Stewart and E. P. Greenberg, *Science*, 1999, **284**, 1318–1322.
3 H.-C. Flemming and J. Wingender, *Nat. Rev. Microbiol.*, 2010, **8**, 623–633.
4 S. S. Magill, J. R. Edwards, W. Bamberg, Z. G. Beldavs, G. Dumyati, M. A. Kainer, R. Lynfield, M. Maloney, L. McAllister-Hollod, J. Nadle, S. M. Ray, D. L. Thompson, L. E. Wilson and S. K. Fridkin, *N. Engl. J. Med.*, 2014, **370**, 1198–1208.
5 P. S. Stewart and J. W. Costerton, *Lancet*, 2001, **358**, 135–138.
6 D. Davies, *Nat. Rev. Drug Discovery*, 2003, **2**, 114–122.
7 D. McDougald, S. A. Rice, N. Barraud, P. D. Steinberg and S. Kjelleberg, *Nat. Rev. Microbiol.*, 2012, **10**, 39–50.
8 H. Wolfmeier, D. Pletzer, S. C. Mansour and R. E. W. Hancock, *ACS Infect. Dis.*, 2018, **4**, 93–106.
9 C. de la Fuente-Núñez, F. Reffuveille, L. Fernández and R. E. W. Hancock, *Curr. Opin. Microbiol.*, 2013, **16**, 580–589.
10 C. de la Fuente-Núñez, F. Reffuveille, K. E. Fairfull-Smith and R. E. W. Hancock, *Antimicrob. Agents Chemother.*, 2013, **57**, 4877–4881.
11 S.-A. Alexander, C. Kyi and C. H. Schiesser, *Org. Biomol. Chem.*, 2015, **13**, 4751–4759.

12 N. Barraud, D. J. Hassett, S.-H. Hwang, S. A. Rice, S. Kjelleberg and J. S. Webb, *J. Bacteriol.*, 2006, **188**, 7344–7353.

13 N. Barraud, M. J. Kelso, S. A. Rice and S. Kjelleberg, *Curr. Pharm. Des.*, 2015, **21**, 31–42.

14 F. Cutruzzolà and N. Frankenberg-Dinkel, *J. Bacteriol.*, 2015, **198**, 55–65.

15 D. P. Arora, S. Hossain, Y. Xu and E. M. Boon, *Biochemistry*, 2015, **54**, 3717–3728.

16 K.-A. Hansen and J. P. Blinco, *Polym. Chem.*, 2018, **9**, 1479–1516.

17 N. R. B. Boase, M. D. T. Torres, N. L. Fletcher, C. de la Fuente-Núñez and K. E. Fairfull-Smith, *Polym. Chem.*, 2018, **9**, 5308–5313.

18 A. D. Verderosa, C. de la Fuente-Núñez, S. C. Mansour, J. Cao, T. K. Lu, R. E. W. Hancock and K. E. Fairfull-Smith, *Eur. J. Med. Chem.*, 2017, **138**, 590–601.

19 C. S. Gudipati, J. A. Finlay, J. A. Callow, M. E. Callow and K. L. Wooley, *Langmuir*, 2005, **21**, 3044–3053.

20 C. Rodriguez-Emmenegger, A. Decker, F. Surman, C. M. Preuss, Z. Sedláková, N. Zydziak, C. Barner-Kowollik, T. Schwartz and L. Barner, *RSC Adv.*, 2014, **4**, 64781–64790.

21 Z. K. Zander and M. L. Becker, *ACS Macro Lett.*, 2018, **7**, 16–25.

22 E. M. Hetrick and M. H. Schoenfisch, *Chem. Soc. Rev.*, 2006, **35**, 780–789.

23 T. N. Gevrek, K. Yu, J. N. Kizhakkedathu and A. Sanyal, *ACS Appl. Polym. Mater.*, 2019, **1**, 1308–1316.

24 H. C. Neu, *Science*, 1992, **257**, 1064–1073.

25 Q. Wei and R. Haag, *Mater. Horiz.*, 2015, **2**, 567–577.

26 D. Y. Ryu, K. Shin, E. Drockenmuller, C. J. Hawker and T. P. Russell, *Science*, 2005, **308**, 236–239.

27 Q. Ye, F. Zhou and W. Liu, *Chem. Soc. Rev.*, 2011, **40**, 4244–4258.

28 B. P. Lee, P. B. Messersmith, J. N. Israelachvili and J. H. Waite, *Annu. Rev. Mater. Res.*, 2011, **41**, 99–132.

29 J. H. Waite and M. L. Tanzer, *Science*, 1981, **212**, 1038–1040.

30 C. Rodriguez-Emmenegger, C. M. Preuss, B. Yameen, O. Pop-Georgievski, M. Bachmann, J. O. Mueller, M. Bruns, A. S. Goldmann, M. Bastmeyer and C. Barner-Kowollik, *Adv. Mater.*, 2013, **25**, 6123–6127.

31 H. Lee, S. M. Dellatore, W. M. Miller and P. B. Messersmith, *Science*, 2007, **318**, 426–430.

32 H. Woehlk, J. Steinkoenig, C. Lang, L. Michalek, V. Trouillet, P. Krolla, A. S. Goldmann, L. Barner, J. P. Blinco, C. Barner-Kowollik and K. E. Fairfull-Smith, *Langmuir*, 2018, **34**, 3264–3274.

33 B. P. Lee, K. Huang, F. N. Nunalee, K. R. Shull and P. B. Messersmith, *J. Biomater. Sci., Polym. Ed.*, 2004, **15**, 449–464.

34 S. H. Hong, S. Hong, M.-H. Ryou, J. W. Choi, S. M. Kang and H. Lee, *Adv. Mater. Interfaces*, 2016, **3**, 1500857.

35 H. Woehlk, J. Steinkoenig, C. Lang, A. S. Goldmann, L. Barner, J. P. Blinco, K. E. Fairfull-Smith and C. Barner-Kowollik, *Polym. Chem.*, 2017, **8**, 3050–3055.

36 J. Liebscher, R. Mrówczyński, H. A. Scheidt, C. Filip, N. D. Hădade, R. Turcu, A. Bende and S. Beck, *Langmuir*, 2013, **29**, 10539–10548.

37 M. d'Ischia, A. Napolitano, A. Pezzella, P. Meredith and T. Sarna, *Angew. Chem., Int. Ed.*, 2009, **48**, 3914–3921.

38 D. Pletzer and R. E. W. Hancock, *J. Bacteriol.*, 2016, **198**, 2572–2578.

39 F. Reffuveille, C. de la Fuente-Núñez, K. E. Fairfull-Smith and R. E. W. Hancock, *Pathog. Dis.*, 2015, **73**, ftv016.

40 X. Du, L. Li, J. Li, C. Yang, N. Frenkel, A. Welle, S. Heissler, A. Nefedov, M. Grunze and P. A. Levkin, *Adv. Mater.*, 2014, **26**, 8029–8033.